Investigation of Submarine Cable Parameters Impact on Energization Transients in Offshore Wind Farms

Ebrahim A. Badran, Mohammad E. M. Rizk, and Mansour H. Abdel-Rahman

***Abstract*— In recent years, many researchers have been involved in investigating the electromagnetic transient phenomena associated with the switching operations in offshore wind farms. It has been reported that, the single core submarine cables are the most distinctive electric component in offshore wind farms. This paper investigates the effect of sheath resistance, semi-conductive layer thickness, and the armor permeability of the single core submarine cables on both transient overvoltages and transformers inrush currents.**

Both transient overvoltages and transformers inrush currents are produced in the offshore wind farm due to the energization of unloaded wind turbine transformers which are connected to each other by single-core submarine cables. The PSCAD/EMTDC program is used for modeling the offshore wind farm. The offshore wind farm investigated in this study consisted of 72 wind turbines arranged in eight rows and each wind turbine is connected to a transformer.

The results show that the transient overvoltage magnitude decreases with increasing the sheath resistance or the armor permeability. The transformer inrush current also decreases with increasing the sheath resistance or the armor permeability.

***Key words* — Offshore Wind Farms, Electromagnetic Transients, Switching Operations, Cable System Energizing, Wind Turbine Transformer Energizing, Capacitor Banks.**

I. Introduction

IN RECENT YEARS, there has been a particular interest in the collection grids of large offshore wind farms. The rapid expansion of the investment in offshore wind farms in many countries has brought problems involving electromagnetic transients to be an important issue. The electrical conditions present in the collection grids are not alike any other electrical grids. The length of medium voltage (MV) submarine cables is remarkable; as well as the number of switchgears and transformers. This combination of components creates an electrical environment never assembled before [1-2].

In the literature, most researches have widely discussed important problems due to switching operations in offshore wind farms. A comparison between measurements, Power Factory and PSCAD/EMTDC simulations of the overvoltages transients due to cable system energizing in Nysted offshore wind farm have been shown in [2]. Measurements and Power Factory simulations of voltage and current transients were performed on the MV Nysted offshore wind farm in [3]. Very fast transient overvoltages due to cable system energizing and its impact on the transformers were investigated using the PSCAD/EMTDC in [4].

It has been reported that, the single-core submarine cables are the most distinctive electric component in offshore wind farms. This paper investigates the effect of sheath resistance, semi-conductive layer thickness, and the armor permeability of the single-core submarine cables on both transient overvoltages and transformers inrush currents. The PSCAD/EMTDC program is used for modeling the offshore wind farm. The transient overvoltages and transformer inrush currents are generated by a switching operation of a row of unloaded wind turbine transformers. The wind turbine transformers are connected to each other by single-core submarine cables. The effect of the capacitor bank on the transformers inrush current is also investigated in this paper.

II. Description of The Investigated Offshore Wind Farm

Fig. 1 shows the single line diagram of the investigated offshore wind farm. It consists of 72 wind turbines arranged in array of 8 rows which are named from A to H [1-2].

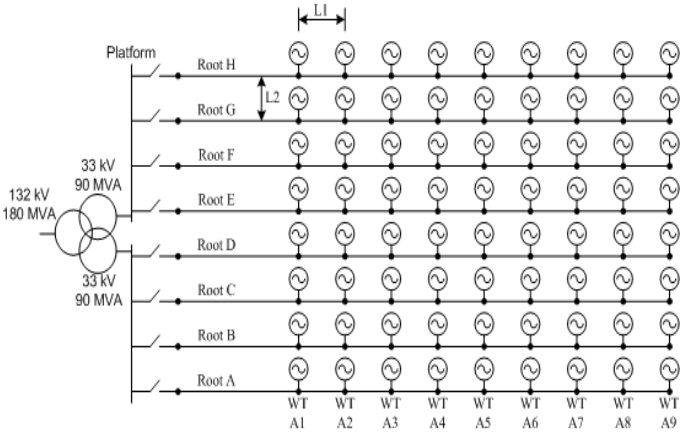

Fig. 1. The offshore wind farm configuration. (L1 = 505 m, L2 = 850 m)

Each wind turbine is rated at 2.3 MW and 0.69 kV and connected to a transformer. The distance between each wind turbine and the adjacent one in each row is 505 m. Each row is separated from the adjacent one by a distance of 850 m. The wind turbine transformers of each row are connected to each other by 33-kV three-phase single-core submarine cables. Each row is then connected to the platform by one root submarine cable. The distance between the platform and last wind turbine (# 9) in the row is 7 km.

Ebrahim A. Badran (ebadran@mans.edu.eg), Mohammad E. M. Rizk (eng_mohammad_2007@mans.edu.eg), and Mansour H. Abdel-Rahman (rahman@mans.edu.eg) are with the electrical Engineering Department, Faculty of Engineering, Mansoura University, Mansoura, Egypt.

The wind farm transformer is rated at 180 MVA and 132/33 kV. It is located in the central position and it has one high voltage winding and two MV windings. Each MV winding is connected to four rows as shown in Fig. 1.

The single-core submarine cables between the wind turbines are connected on the bottom of each wind turbine where the armor and the sheath of the cables are grounded. The wind turbine transformer (WTT) is rated at 2.5 MVA and 33/0.69 kV. It is connected to the submarine cables via a switch disconnecting fuse on the MV side. On the low voltage (LV) side of each transformer only the capacitor bank to compensate the induction generator and a small load are included in the simulations. Furthermore, included in the wind farm model is the connection of the wind farm transformer via a single three-phase high voltage (HV) submarine (sea) cable (132 kV /10.5 km) and underground cable (132 kV /18.3 km) to the grid connection point on land.

III. Modeling of The Electric Components of The Offshore Wind Farm using THE PSCAD/EMTDC

In this section, the detailed modeling of the electric components of the offshore wind farm using the PSCAD/EMTDC is demonstrated. These components include submarine cables, transformers, power system grid, and capacitor banks.

a) System Modeling for Switching Study

Fig. 2 shows the PSCAD/EMTDC model of the offshore wind farm. In this model, it is shown that:

(*i*) The grid is modeled as a voltage source.

(*ii*) the HV, 132-kV, three-phase single-core cables are modeled using the equivalent PI sections.

(*iii*) The wind farm transformer is modeled as three winding transformer using the classical model approach.

(*iv*) The rows E, F, G, and H are modeled as one three-phase single-core cables because they are connected in parallel. Also, the rows B,C, and D are modeled in the same way.

Only row A is modeled in details as shown in Fig. 2. The nine WTTs in row A are the same but only WTT#1 has a capacitor bank connected at its LV side. This connected capacitor bank is modeled to show its effect on the transformer inrush current. A very light load is connected on the LV side of the nine wind turbine transformers. The light load is modeled as a resistance of 1200 Ω. So, the nine WTTs are treated as no loaded transformers.

b) Cable Parameters Calculation

The MV single core submarine cables are the most distinctive electric component in the offshore wind farms. The geometric configuration of the 33 kV three-phase single-core submarine cables between the wind turbine transformers is calculated based on the power transferred through them [5], and given in Table 1.

In submarine cables, the armor is usually quite thick [6]. Therefore, it is assumed in this study that, an armor of 5 mm steel wires thickness and a 5 mm outer insulation thickness are incorporated into the three-phase single-core submarine cable design. So, the overall outer diameter of the cable is 65 mm. Fig. 3 shows the geometric configuration of the MV submarine cable.

The MV 33-kV submarine cables, , are modeled using the frequency dependent (phase) model. This model represents the frequency dependence of internal transformation matrices [10].

The HV, 132 kV sea and land cables, are modeled using the PI equivalent sections to avoid the numerical errors due to the long length of the HV cables. The PI equivalent parameters are calculated from the cable geometric dimensions and its materials using Bergeron model at 50 Hz. Table 2 gives both positive and zero sequence resistance, inductive and capacitive reactance of the 132-kV sea and land cables in the wind farm.

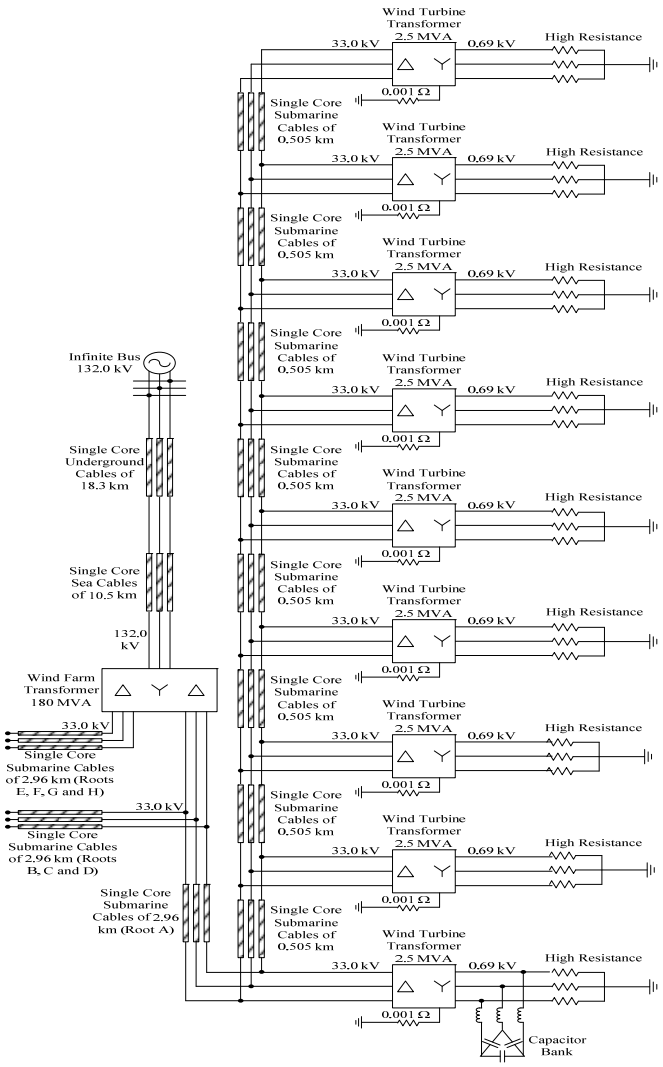

Fig. 2. The offshore wind farm PSCAD/EMTDC model.

The cable core data entries for the PSCAD/EMTDC are manipulated as explained in [7]. The main insulation of high voltage cables is based on extruded insulation type and is always sandwiched between two semiconductive layers. Unfortunately, the PSCAD/EMTDC does not allow the user to directly specify the semiconducting layers [8-9]. These must, therefore, be introduced by a modification of the input data by allowing the insulation to extend between the core conductor

and sheath conductor, and increasing the permittivity proportionally to leave the capacitance unaltered.

The semi-conductive layer thickness is computed as given in [7] – [9]. Both core and sheath of the submarine cable are made of copper. The resistivity of the surrounding ground depends strongly on the soil characteristics. The resistivity of sea water lies between 0.1 and 1 Ω.m [6]. The ground resistivity is assumed to be 1 Ω.m in this study.

Table 1: Geometric Dimensions of the 33-kV Single Core Cable

Cross section of conductor (A_c) [mm]^2	240.0
Diameter of conductor (d_2) [mm]	18.1
Insulation thickness (T_{ins}) [mm]	8.0
Diameter over insulation (Do_{ins}) [mm]	35.7
Cross section of screen (A_{sh}) [mm]^2	35.0
Outer diameter of cable (Do) [mm]	45.0

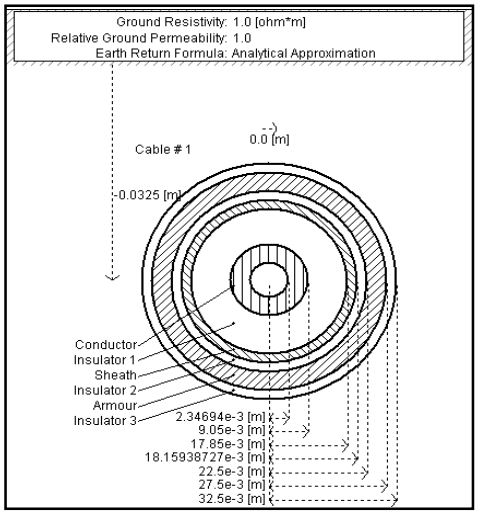

Fig. 3. The MV cables geometric configuration modeled in PSCAD/EMTDC

Table 2 : 132 kV Single Core Cables Data at 50 Hz

The 132 kV land cable (equivalent PI section model)	
length	18300.0 [m]
+ve sequence resistance	0.0870615666 [m ohm/m]
+ve sequence inductive reactance	0.122644966 [m ohm/m]
+ve sequence capacitive reactance	9.091530621 [M ohm*m]
zero sequence resistance	0.186524753 [m ohm/m]
zero sequence inductive reactance	0.0551011310 [m ohm/m]
zero sequence capacitive reactance	9.091530621 [M ohm*m]
The 132 kV sea cable (equivalent PI section model)	
length	10500.0 [m]
+ve sequence resistance	0.0863663070 [m ohm/m]
+ve sequence inductive reactance	0.122711970 [m ohm/m]
+ve sequence capacitive reactance	9.091530621 [M ohm*m]
zero sequence resistance	0.182742143 [m ohm/m]
zero sequence inductive reactance	0.0619589991 [m ohm/m]
zero sequence capacitive reactance	9.091530621 [M ohm*m]

c) Transformer Modeling

PSCAD/EMTDC offers two different transformer models when it comes to the saturation modeling. The first model is the classical modeling approach which does not take into account the magnetic coupling between different phases. The second model is the unified magnetic equivalent circuit (UMEC) transformer models which are based primarily on core geometry. For the transformer model based on the UMEC algorithm, phases are magnetically coupled [10].

The air core reactance for the classical model approach is chosen as twice the positive sequence leakage reactance [11].

d) Capacitor Bank Modeling

The capacitor bank is connected to the LV side of the WTT. It is utilized to compensate for the reactive consumption of the asynchronous machine under generation.

It is a common use in the capacitor banks to include a reactor before the capacitors in order to protect the banks. In this situation, the reactor is indirectly defined by the degree of inductance in the capacitor bank. This degree represents the ratio between the inductive and capacitive reactance of the equipment. The reactance and capacitance in the capacitor bank can be calculated if the reactive power generation, the nominal frequency and the voltage on the LV side of the WTT are known [1].

IV. Switching Transients Analysis

In this section, the impact of the single-core submarine cable parameters is investigated for both transient overvoltages and wind turbine transformers inrush currents. This is carried out by energizing of row which consists of nine wind turbines transformers which are connected to each other by single-core submarine cables. The impact of the single-core submarine cable parameters; sheath resistance, semi-conductive layers thickness, and permeability of the armor are investigated.

For transient overvoltages investigation, the energization is performed by switching phase A at peak voltage instant. This switching instant represents the worst case of the energization of a cable system. Thus, it results in maximum magnitude of transient overvoltage [12-13].

Furthermore, the inrush currents resulting from energizing the unloaded wind turbine transformers of row A is studied. In this case, the switching operation is performed at phase A voltage zero cross point. This switching instant represents the worst case as it results in maximum magnitude of inrush currents [12-13].

a. Impact of the Cable Sheath Resistance

The effect of the cable sheath resistance is investigated. Two sheath resistances are discussed. The first case is a copper sheath with inner radius of 17.85 mm and outer radius of 18.1594 mm. The second case is a lead sheath with inner radius of 17.85 mm and outer radius of 18.85 mm. The dc resistance of the copper sheath is 0.49143 mΩ/m and 1.908125 mΩ/m for the lead sheath.

Fig. 4 shows the transient overvoltage waveforms of phase A after the circuit breaker closure instant. The comparison between the overvoltage at the two sheath cases is illustrated at the high voltage side of the two wind turbine transformers; WTT#1 and WTT#9.

It is clearly seen that, an increase in cable sheath resistance results in a decrease in the transient overvoltage magnitude. This is due to the attenuation in the traveling transient voltage waves. The effect of sheath resistance on peak values of the transient overvoltages at both WTT#1 and WTT#2 is given in Table 3. Furthermore, the propagation speed of the transient voltage waves is the same with changing the sheath resistance.

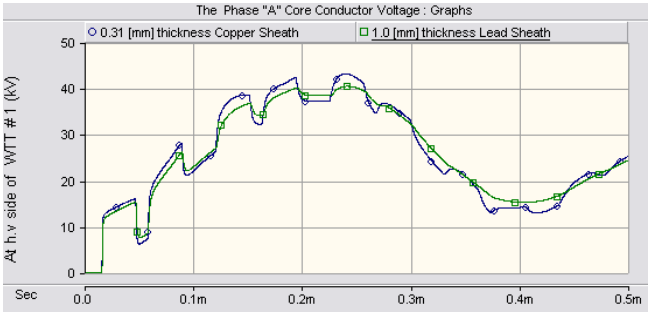

(a) At WTT 1

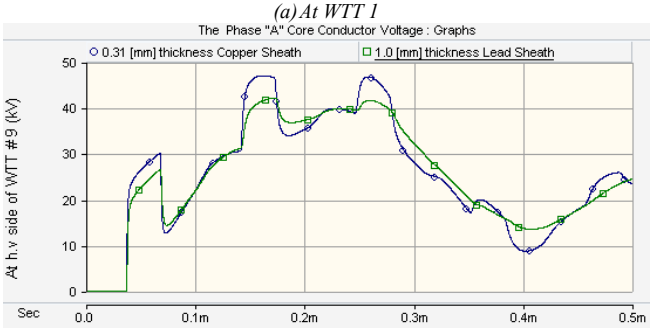

(b) At WTT 9

Fig. 4. Transient overvoltage waveforms of phase A for two cable sheath resistances

Also, it can be noted the duplication in the transient voltage at WTT#9 due to the reflection of the transient voltage wave at the open ended cable. Whereas, the transient voltage reaches 15 kV at WTT#1 and 30 kV at WTT#9 for copper sheath case. This is due to the difference between the traveling time of the transient voltage wave from the plat form where the switching operation is done to WTT#1 and WTT#9.

Fig. 5 shows the wind turbine transformer inrush current waveforms of phase A after the circuit breaker closure. The comparison between the wind turbine transformer inrush current waveforms for the two sheath cases is illustrated at the high voltage side of the two wind turbine transformers; WTT#1 and WTT#9.

It is shown that, an increase in cable sheath resistance results in a decrease in the magnitude of the wind turbine transformer inrush current. The effect of sheath resistance on peak values of the wind turbine transformers inrush currents at both WTT#1 and WTT#2 is given in Table 3. The percentage increase in the transformer inrush current due to the decrease in cable sheath resistance is more significant when the transformer position is far from the switched circuit breaker.

Also, it is shown the effect of the capacitor bank because there is small capacitor inrush current which is superposed on the WTT#1 inrush current. This capacitor inrush current is small because the switching operation is done at the zero crossing point on phase A voltage waveform. So the effect of the capacitor inrush current is more significant in the inrush current of the two other phases.

Table 3: Effect of the sheath resistance on the peak values of transient overvoltages and transformers inrush currents.

		Copper Sheath (0.49143 mΩ/m)	Lead Sheath (1.908125 mΩ/m)
At WTT # 1	[kV]	43.177	40.446
	[A]	123.11	114.01
At WTT # 9	[kV]	47.022	42.163
	[A]	110.65	95.17

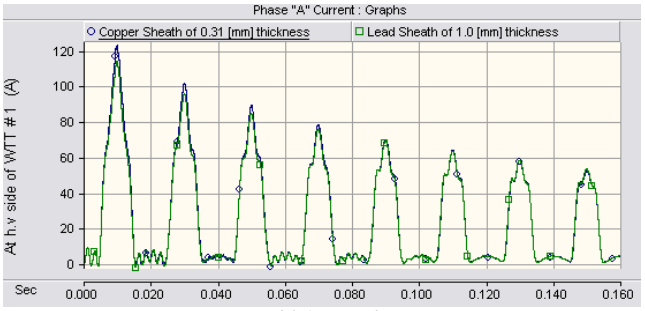

(a) At WTT 1

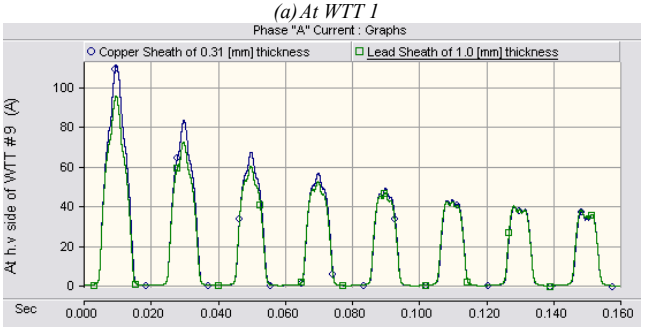

(b) At WTT 9

Fig. 5. Phase A wind turbine transformer inrush current waveforms with two different cable sheath resistances

b. Impact of the Cable Semi-conductive layers Thickness

In this section, the effect of cable semi-conductive layer thickness is investigated as two different cable semi-conductive layer thickness cases are analysed. The first case is 0.8 mm thickness and the second case is 3.0 mm thickness.

Fig. 6 shows the transient overvoltage waveforms of phase A after the circuit breaker closure instant. The comparison between the overvoltage for the two different cable semi-conductive layer thickness cases at the high voltage side of the two wind turbine transformers; WTT#1 and WTT#9.

It is shown that, an increase in cable semi-conductive layers thicknesses results in a decrease in the propagation speed of the transient voltage waves. This can be attributed to that with a fixed main insulation thickness, adding semi-conductive layers increases the inductance of the core - sheath loop without changing the capacitance. The magnitude of the

transient voltage waves is nearly the same with changing the semi-conductive layers thickness in the cable.

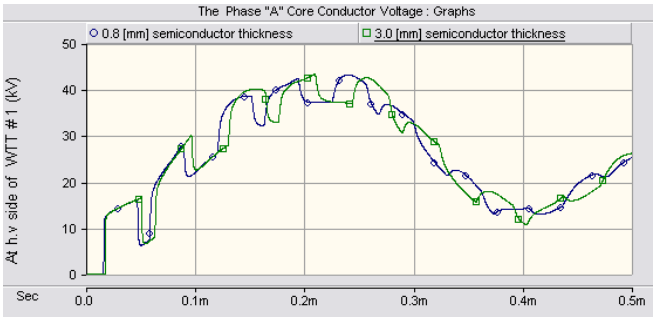

(a) At WTT 1

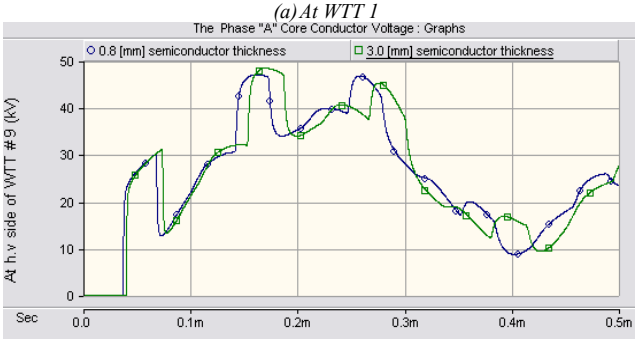

(b) At WTT 9

Fig. 6. Phase A transient overvoltage waveforms with two different cable semi-conductive layers thicknesses

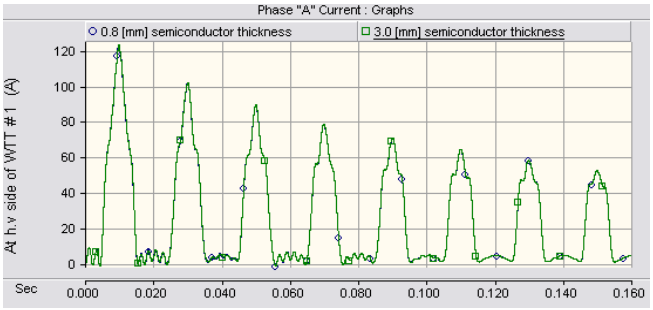

(a) At WTT 1

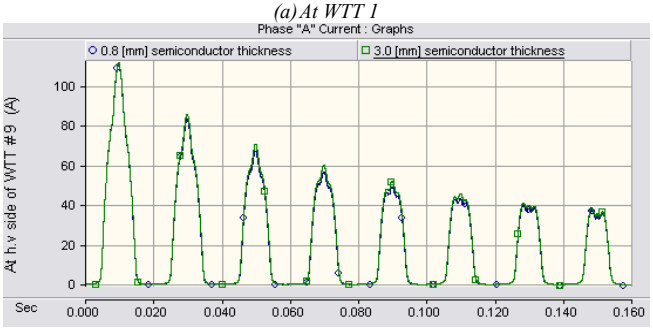

(c) At WTT 9

Fig. 7. Phase A wind turbine transformer inrush current waveforms with two different cable semi-conductive layers thicknesses

Fig. 7 shows the wind turbine transformer inrush current waveforms of phase A after the circuit breaker closure. The comparison between the wind turbine transformer inrush current waveforms for the two different semi-conductive layers thicknesses cases is illustrated at the high voltage side of the two wind turbine transformers; WTT#1 and WTT#9.

It is clearly seen that, the change in the semi-conductive layers thicknesses in the single core submarine cables has no effect on the magnitude of the wind turbine transformers inrush current. The effect of the capacitor bank on the inrush current waveform at WTT#1 is obvious.

c. Impact of the Armor Permeability

In this section, the impact of armor permeability is investigated. Two different cable armor permeability are studied. The first relative permeability of the cable armor is 1.0 and the second is 400. Each value of the cable armor relative permeability is studied at two sheath cases. The first is a copper sheath with 17.85 mm inner radius and 18.1594 mm outer radius. The second is a lead sheath with 17.85 mm inner radius and 18.85 mm outer radius.

Fig. 8 shows the transient overvoltage waveforms of phase A after the circuit breaker closure instant for the comparison between the transient overvoltage for the two different cable armor relative permeability cases with lead sheath at the high voltage side of the two wind turbine transformers; WTT#1 and WTT#9.

It is seen that, an increase in cable armor permeability results in a decrease in the magnitude of the transient overvoltages. The effect of armor permeability on peak values of the transient overvoltages for lead sheath at both WTT#1 and WTT#2 is given in Table 4.

The propagation speed of the transient voltage waves nearly the same with changing the relative permeability of the cable armor. The percentage increase in the magnitude of the transient overvoltages due to the decrease in the relative permeability of the cable armor is more significant wherever the transformer position is far from the circuit breaker which has been closed.

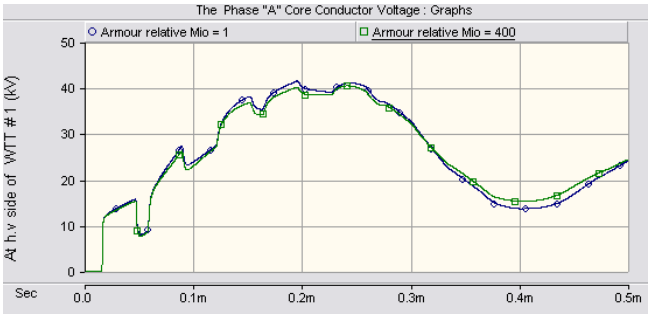

(a) At WTT 1

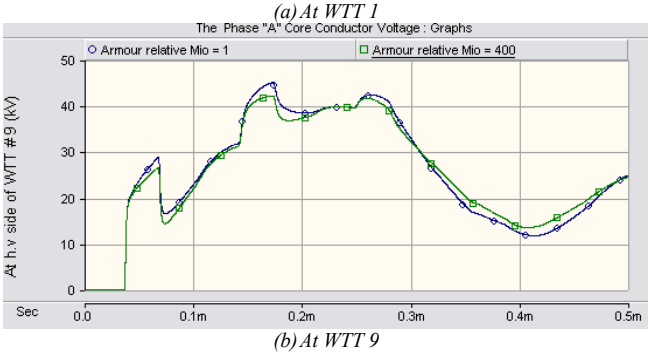

(b) At WTT 9

Fig. 8. Phase A transient overvoltage waveforms with two different cable armor relative permeability (lead sheath case)

Fig. 9 shows the comparison between the transient overvoltage for the two different cable armor relative permeability cases with copper sheath at the high voltage side

of the two wind turbine transformers; WTT#1 and WTT#9. It is clearly seen that, there is no difference in the transient overvoltage waveforms with changing the relative permeability of the cable armor between 1 and 400. The effect of armor permeability on peak values of the transient overvoltages for copper sheath at both WTT#1 and WTT#2 is given in Table 4.

The significance of the submarine cable armor permeability is arises when the magnetic field penetrates the cable sheath (*i.e* the sheath layer penetration depth of magnetic field is more than the sheath thickness). In this case, the magnetic field causes interaction with the armor layer. The penetration depth δ of the magnetic field in a conductive material is determined from [14];

$$\delta = \sqrt{\frac{2}{\omega\mu\sigma}} \quad [\text{m}] \qquad (1)$$

where ω is the magnetic field frequency, μ is the permeability of the conductive material, and σ is the conductivity of the material.

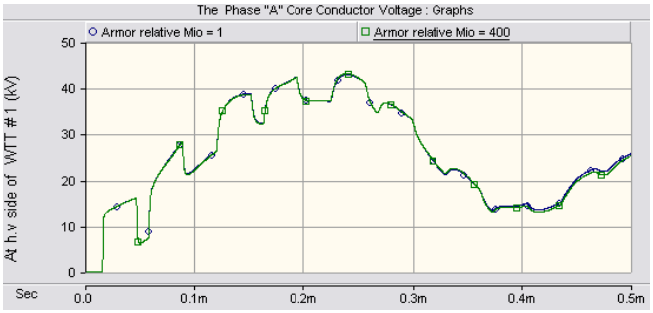

(d) At WTT 1

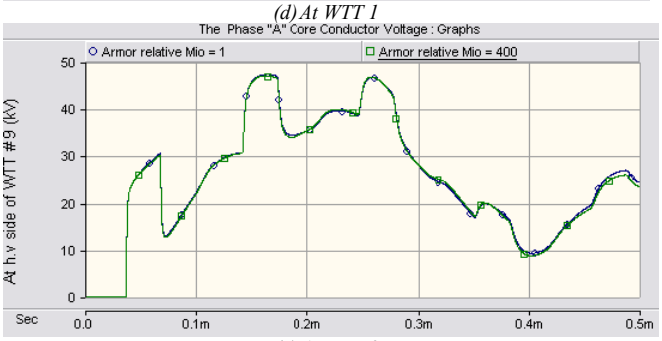

(e) At WTT 9

Fig. 9. Phase A transient overvoltage waveforms with two different cable armor relative permeability (copper sheath case)

Fig. 10 shows the wind turbine transformer inrush current waveforms of phase A after the circuit breaker closure. The comparison between the wind turbine transformer inrush current waveforms for the two different cable armor relative permeability for lead sheath case is illustrated at the high voltage side of the two wind turbine transformers; WTT#1 and WTT#9.

It is shown that, an increase in cable armor permeability results in a decrease in the magnitude of the wind turbine transformer inrush current. The effect of armor permeability on peak values of the wind turbine transformers inrush currents for lead sheath at both WTT#1 and WTT#2 is given in Table 4. Fig. 11 shows the comparison between the wind turbine transformer inrush current waveforms for the two different cable armor relative permeability for copper sheath case at the high voltage side of the two wind turbine transformers; WTT#1 and WTT#9.

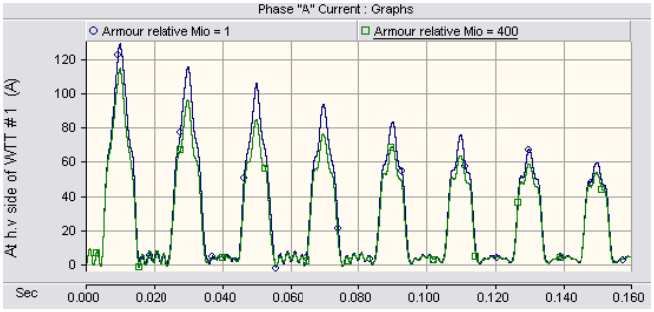

(a) At WTT 1

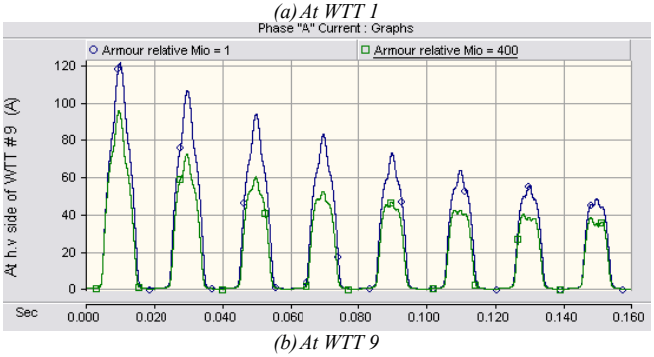

(b) At WTT 9

Fig. 10. Phase A wind turbine transformer inrush current waveforms with two different cable armor relative permeability at (lead sheath case)

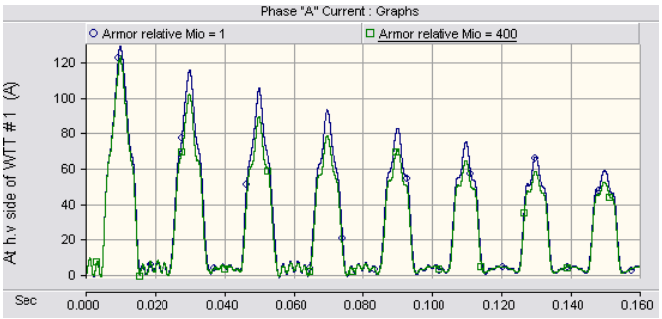

(a) At WTT 1

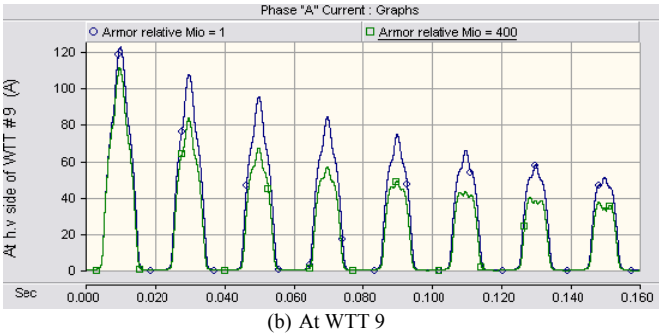

(b) At WTT 9

Fig. 11. Phase A wind turbine transformer inrush current waveforms with two different cable armor relative permeability (copper sheath case)

It is shown that, an increase in cable armor permeability results in a decrease in the magnitude of the wind turbine transformer inrush current. The effect of armor permeability on peak values of the wind turbine transformers inrush

currents for copper sheath at both WTT#1 and WTT#2 is given in Table 4.

Table 4: Effect of the armor permeability on the peak values of transient overvoltages and transformers inrush currents.

		Copper Sheath		Lead Sheath	
		$\mu_r = 1$	$\mu_r = 400$	$\mu_r = 1$	$\mu_r = 400$
At WTT # 1	[kV]	43.177	43.177	41.477	40.446
	[A]	128.93	123.11	128.78	114.01
At WTT # 9	[kV]	47.022	47.022	45.047	42.163
	[A]	122.16	110.65	121.19	95.17

It is clearly seen that, the percentage of increase in wind turbine transformer inrush current due to the decrease in cable armor relative permeability is more significant whenever the transformer position is far from the circuit breaker which has been closed. Also, the percentage of increase in wind turbine transformer inrush current due to the decrease in cable armor relative permeability is more significant at the case of lead sheath than copper sheath. This can be attributed to that the conductivity of lead is much less than the copper so the penetration depth in lead is more than copper and then the effect of changing the armor permeability is more significant.

In spite of the impact of the submarine cable armor permeability on the transient overvoltages is not clear in the case of copper sheath, it is rather clear in the case of transformers inrush current. This can be attributed to that the frequency content of the transformers inrush currents is very low order frequency with respect to the frequency of the transient overvoltages. As the penetration depth is inversely proportional to the frequency so the effect of armor is clear for the transformers inrush currents and not for the transient overvoltages.

V. Conclusion

This paper investigates the effect of sheath resistance, semi-conductive layer thickness and the armor permeability of the single core submarine cables on both transient overvoltages and transformers inrush currents in offshore wind farms.

The results show that, the increase in the resistance of the sheath has no effect on the propagation velocity of the transient overvoltages and results in a decrease in both the transient over voltage and the transformer inrush current. The effect of the cable sheath resistance is on both the transient over voltage and the transformers inrush currents is more significant whenever the transformer position is far from the circuit breaker which has been closed.

Also, it has been showed that the increase in the semi-conductive layer thickness results in a decrease of the propagation velocity of the transient overvoltage waveforms and has no effect on the magnitude of transformer inrush current.

The effect of the armor permeability is also investigated at two cases of copper sheath and lead sheath. The results show that the decrease in armor permeability results in an increase in the magnitude of the transient overvoltages. This effect is only significant if the electromagnetic waves can penetrate the sheath so the armor effect is clear with the lead sheath case and not clear for the copper sheath case. The decrease in armor permeability results in an increase in the magnitude of transformer inrush current also. The percentage of the increase in the magnitude of transformer inrush current is more with lead sheath case than copper sheath case.

References

[1] Iván Arana Aristi, "Modeling of Switching Transients in Nysted Offshore Wind Farm and a Comparison with Measurements", M.Sc. Thesis, June 2008, Technical University of Denmark.

[2] I. Arana, J. Holbøll, T. Sørensen, A. H. Nielsen, P. Sørensen, and O. Holmstrøm, "Comparison of Measured Transient Overvoltages in the Collection Grid of Nysted Offshore Wind Farm with EMT Simulations", International Conference on Power Systems Transients, IPST2009, Kyoto, Japan, June 3-6, 2009.

[3] Poul Sørensen, Anca D. Hansen, Troels Sørensen, Christian S. Nielsen, Henny K. Nielsen, Leif Christensen, and Morten Ulletved, "Switching transients in wind farm grids", available at www.ewec2007.

[4] Lars Liljestrand, Ambra Sannino, Henrik Breder, and Stefan Thorburn, "Transients in Collection Grids of Large Offshore Wind Parks", Wind Energy, Wiley Interscience, 2008, pp. 45–61.

[5] "ABB XLPE Cables User's Guide", Technical documentation, available at www.abb.com.

[6] J. A. Martinez, B. Gustavsen, and D. Durbak, "Parameter Determination for Modeling System Transients - Part II: Insulated Cables," IEEE Transactions on Power Delivery, Vol. 20, No. 3, July 2005, pp. 2045-2050.

[7] Abey Daniel and Samson Gebre, "Analysis of Transients in Wind Parks: Modeling of System Components and Experimental Verification", M.Sc. Thesis, Chalmers University of Technology, Göteborg, Sweden, 2008.

[8] Daniel Mireanu, "Transient Over-voltages in Cable Systems - Part 1 : Theoretical Analysis of Large Cable Systems", M.Sc. Thesis, Chalmers University of Technology, Göteborg, Sweden, 2007.

[9] Maialen Boyra, "Transient Overvoltages in Cable Systems - Part 2 : Experiments on Fast Transients in Cable Systems," M.Sc. Thesis, Chalmers University of Technology, Göteborg, Sweden, 2007.

[10] "PSCAD/EMTDC USER'S GUIDE," Manitoba HVDC Research Centre, 2005.

[11] Mukesh Nagpal, Terrence G. Martinich, Ali Moshref, Kip Morison, and P. Kundur, "Assessing and Limiting Impact of Transformer Inrush Current on Power Quality", IEEE Transactions on Power Delivery, Vol. 21, No. 2, April 2006, pp. 890-896.

[12] A. Greenwood, "Electrical Transients in Power Systems", 2nd Edition, Wiley Interscience, 1991.

[13] Lou van der Sluis, "Transients in Power Systems", John Wiley & Sons Ltd., 2001

[14] Juan A. Martinez-Velasco, "Power System Transients – Parameters Determination", Taylor and Francis Group, LLC., 2010.